Smart Structures and Systems, *Vol. 30, No. 1 (2022) 89-106*
https://doi.org/10.12989/sss.2022.30.1.089

Optimal design of a viscous inertial mass damper for a taut cable by the fixed-points method

Y.F. Duan, S.H. Dong, S.L. Xu* and C.B. Yun

College of Civil Engineering and Architecture, Zhejiang University, China

(*Received June 25, 2021, Revised November 21, 2021, Accepted December 15, 2021*)

Abstract. The negative stiffness of an active or semi-active damper system has been proven to be very effective in reducing dynamic response. Therefore, energy dissipation devices possessing negative stiffness, such as viscous inertial mass dampers (VIMDs), have drawn much attention recently. The control performance of the VIMD for cable vibration mitigation has already been demonstrated by many researchers. In this paper, a new optimal design procedure for VIMD parameters for taut cable vibration control is presented based on the fixed-points method originally developed for tuned mass damper design. A model consisting of a taut cable and a VIMD installed near a cable end is studied. The frequency response function (FRF) of the cable under a sinusoidal load distributed proportionally to the mode shape is derived. Then, the fixed-points method is applied to the FRF curves. The performance of a VIMD with the optimal parameters is subsequently evaluated through simulations. A taut cable model with a tuned VIMD is established for several cases of external excitation. The performance of VIMDs using the proposed optimal parameters is compared with that in the literature. The results show that cable vibration can be significantly reduced using the proposed optimal VIMD with a relatively small amount of damping. Multiple VIMDs are applied effectively to reduce the cable vibration with multi-modal components.

Keywords: cable vibration control; fixed-points method; mode split; multi-mode control; multiple VIMDs; optimal design; viscous inertial mass damper

1. Introduction

Cables are widely used in cable-supported bridges and long-span structures due to their economy, beauty, and light weight. However, cables are prone to severe vibration because of their low inherent damping and high flexibility and this vibration can be detrimental to the serviceability and safety of the structures.

As an effective measure, installing external dampers is widely used in vibration suppression of stay cables. However, the conventional passive viscous damper offers limited control performance because the achievable maximum system damping is limited and approximately proportional to the distance between the damper and the cable anchorage (Kovacs 1982, Pacheco *et al*. 1993, Krenk 2000, Krenk and Nielsen 2002, Fujino and Hoang 2008). Hence, semi-active dampers were numerically (Johnson *et al*. 1999a, b, Jamshidi *et al*. 2017) and experimentally (Ni *et al*. 2002, Christenson *et al*. 2015) investigated during the past few decades. As a typical semi-active device, it has been proven that magneto-rheological dampers can provide very effective cable vibration mitigation (Spencer *et al*. 1997, Jeong *et al*. 2019, Duan *et al*. 2019a, b). One of the reasons for this is their negative stiffness (Li *et al*. 2008, Iemura and Pradono 2010, Høgsberg *et al*. 2011, Weber and Distl 2015, Bahar *et al*. 2018). Therefore, energy dissipation devices possessing the property of negative stiffness, such as viscous inertial mass dampers (VIMDs), have drawn much attention recently (Shi and Zhu 2015, Javanbakht *et al*. 2018, Lu *et al*. 2019). Garrido *et al*. (2013) proposed a novel inerter-based damper, rotational inertia double-tuned mass damper (RIDTMD), and presented the optimum design parameters. Nakamura *et al*. (2014) presented a type of electromagnetic inertial mass damper (EIMD) and showed that it could reduce both acceleration and displacement. Lu *et al*. (2017) determined the optimal VIMD parameters for a taut cable by using the Galerkin method and the state-space formulation. Shi and Zhu (2018) investigated the dynamic characteristics of an inerter-based negative stiffness damper using complex modal analysis, and gave an optimal design procedure based on wavenumber analysis.

Den Hartog (1934) found that the frequency response function (FRF) curve of a structure with a dynamic vibration absorber (DVA) or a tuned mass damper (TMD) passes through two fixed points, which are independent of the damping, and thereby proposed a fixed-points method (FPM) to optimize the DVA parameters. This method is separated into two steps. The absorber frequency should be well tuned, making the dynamic amplitudes of the FRF curves at the two fixed points equal. Then the damping ratio can be selected to make the slope of the FRF curve horizontal at the fixed points, so that the FRF may have the same maximum amplitude at the points. Brock (1946) proposed another approach to obtain the optimal damping,

*Corresponding author, Ph.D., Professor,
E-mail: slxu@zju.edu.cn

ISSN: 1738-1584 (Print), 1738-1991 (Online)

by forming a flat plateau on the FRF curve between two fixed points. Ren (2001) applied the FPM on a new type of DVA, whose damping element was directly connected to the ground. Krenk (Krenk 2005, Krenk and Høgsberg 2009) derived the optimal parameters of an additional TMD for an undamped SDOF system using the FPM, and proposed a combined design method which was based on the FPM for flexible structures. Ozer and Royston (2005) extended the classical Hartog's approach for a damped MDOFs system with TMDs. Liu and Liu (2005) claimed that they had failed to obtain any results by the original fixed-points method (differentiating FRF), but that they were able to obtain a detailed derivation for a skyhook damper with Brock's approach. Furthermore, Shum (2009) applied this method on a tuned liquid column damper to suppress harmonic vibration of structures. Ikago *et al*. (2012a, b) studied the performance of viscous mass damper (VMD) on SDOF and MDOF structures with using the fixed-points method, respectively. Marian and Giaralis (2017) optimized the parameters of the tuned mass-damper-inerter (TMDI) by application of Den Hartog's tuning approach (FPM) and showed that the TMDI is more effective from a same mass TMD. Wong *et al*. (2018) investigated the viscoelastic dynamic vibration absorber (VDVA), and gave the optimal parameters based on the modified fixed-points method. Shen *et al*. (2017) proposed the optimal analytical parameters of a DVA with negative stiffness. Zhu *et al*. (2018) studied the analytical optimization formulas of a DVA for mitigating vibration of a plate using the fixed-points theory. Hua *et al*. (2018) applied this method on a beam and proposed a design guideline. A negative stiffness amplifying damper (NSAD) was studied by Wang *et al*. (2019), and the authors presented closed-form expressions of the optimal NSAD parameters for an undamped SDOF system, based on the fixed-points theory. Recently, Batou and Adhikari (2019) presented an analytical approach to obtain the optimal parameters of a viscoelastic TMD using the fixed-point method.

The new optimization method of VIMD for vibration control of taut cables that we present in this paper is based on the fixed-points method and differs from the existing research. We extended the FPM to the real cable system and optimized the VIMD by directly reducing the structural response, while the existing damper optimizations for cables aimed at obtaining a high modal damping ratio. We derived the FRF of a cable under a sinusoidal load distributed proportionally to the mode shape. We also found the mode split phenomenon of a cable with a VIMD and analyzed it in depth. We developed the optimal design procedures for the VIMD, obtained the corresponding optimal parameters, and carried out simulations for a taut cable-VIMD system. The performance of the optimal VIMD was investigated for several load cases, i.e., concentrated harmonic load, and three distributed loads of band-limited Gaussian white noise, earthquake load, and wind load. We analyzed the simulation results and compared them with those using other types of damper in literatures. Finally, we applied multiple VIMDs to the cable vibration reduction under the excitations with multi-modal components.

(a) Ball-screw

(b) Rack-pinion

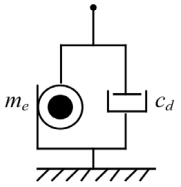

(c) Schematic of a VIMD

Fig. 1 Inerters and schematic of the VIMD

2. VIMDs on ordinary structures and on cables

2.1 A VIMD on an ordinary structure

A viscous inertial mass damper (VIMD) consists of an inertial mass element and a viscous damping element. The inertial mass element uses a mechanical device such as a ball-screw or a rack-pinion to convert translational motion to rotational motion (Fig. 1), so that the effective inertial mass m_e can be amplified tenfold or even a hundredfold, as in Eq. (1)

$$m_e = r^2 I \tag{1}$$

where m_e is the effective inertial mass, I is the mass moment of inertia, and r^2 is the converting factor.

Another advantage of a VIMD is that the static response of the system will not be affected by the inerter due to its small real mass. A simplified mechanism for a VIMD is shown in Fig. 1(c), where c_d is the viscous damping coefficient.

The damper force F_d of a VIMD can be expressed as

$$F_d = m_e \ddot{x} + c_d \dot{x} \tag{2}$$

where $\ddot{x}$ and $\dot{x}$ are the relative acceleration and velocity between two terminals of a VIMD. Assuming the motion x is harmonic with $x = e^{i\omega t}$ and ω is the exciting frequency, Eq. (2) becomes

$$F_d = -\omega^2 m_e e^{i\omega t} + i\omega c_d e^{i\omega t} \tag{3}$$

The first term in Eq. (3) can be considered as an equivalent negative stiffness, which may cause a slight increase in the structural response. Fig. 2 shows the force-displacement hysteresis loops of a VIMD and a pure VD,

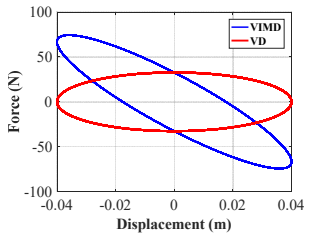

Fig. 2 Force-Displacement relationship of VIMD and VD

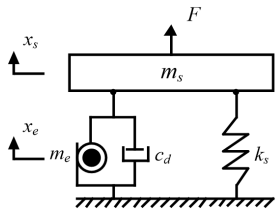

Fig. 3 An ordinary SDOF system with a VIMD

from which the negative stiffness effect of the VIMD can be observed.

For an ordinary SDOF system with a VIMD (Fig. 3), there is no relative displacement between the inertial mass m_e and structural mass m_s: i.e., $x_e = x_s$. Hence, the equation of motion for x_s can be written as

$$(m_s + m_e)\ddot{x}_s + c_d\dot{x}_s + k_s x_s = F \tag{4}$$

where m_s and k_s are the mass and stiffness of the SDOF system; F denotes the external load on m_s; and the structural damping is neglected.

The frequency response function (FRF) of the structural mass can be obtained as

$$H(\omega) = \frac{1}{k_s + ic_d\omega - (m_s + m_e)\omega^2} \tag{5}$$

Fig. 4 shows the FRF curves for various damper parameters. The curves in Fig. 4(a) have the same mass ratio $\mu(= 2.0)$ but different damping ratio ξ, where $\mu = \frac{m_e}{m_s}$, $\xi = \frac{c_d}{2m_s\omega_s}$, and $\omega_s = \sqrt{\frac{k_s}{m_s}}$. In Fig. 4(b), all curves have the same $\xi(= 0.08)$ but different μ. Since the dynamic degree of freedom is not increased, the system still has only one mode after installing a VIMD. This is completely different from the case of a tuned mass damper (TMD), which introduces an additional mode to the system. Fig. 4 clearly shows that the natural frequency is reduced due to the additional inertial mass, whereas the response is suppressed with increased damping.

2.2 A VIMD on a cable

In this study, we analyzed a taut cable with mass per unit length m, tension T, and length L under a distributed external load $f_n(x,t)$ proportional to the target cable mode $\varphi_n(x)$ as shown in Fig. 5. A VIMD was installed at x_d near the left end of the cable. x and x' are a pair of complementary coordinates along the cable. The equation of motion for the cable system can be obtained as

$$m\ddot{y}(x,t) - Ty''(x,t) = F_d(t)\delta(x - x_d) + f_n(x,t) \tag{6}$$

where, $y(x,t)$ is the transverse displacement of the cable; $(\dot{})$ and $(')$ denote partial differentiations with respect to t and x, respectively; $F_d(t)$ is the damper force; $\delta(\cdot)$ is a delta functions; $f_n(x,t)$ is a distributed load assumed to be proportional to the target cable mode $\varphi_n(x)$ as in Eq. (7); and the inherent cable damping and dynamic variation of cable tension are neglected.

$$f_n(x,t) = \tilde{f}_n \cdot e^{i\omega t} \cdot sin\left(\frac{n\pi}{L}x\right), \qquad n = 1,2,3,\ldots \tag{7}$$

Note that the nth natural frequency ω_n and mode $\varphi_n(x)$ of the undamped cable without a VIMD are

$$\omega_n = \frac{n\pi}{L}\sqrt{\frac{T}{m}}, \qquad \varphi_n(x) = sin\left(\frac{n\pi}{L}x\right) \tag{8}$$

The installation of a VIMD results in a discontinuity in the slope of the cable at the damper location x_d. The cable can thus be analyzed by dividing it into two segments, and the equilibrium equation at x_d is obtained as

$$T\left(y'(t)|_{x_d^+} - y'(t)|_{x_d^-}\right) = F_d(t) \tag{9}$$

where the prime $(')$ denotes the differentiation with respect to x.

With the separation of variables method as in the distributed load $f_n(x,t)$ in Eq. (7)

$$y_n(x,t) = \tilde{y}_n(x)e^{i\omega t}, \qquad F_d(t) = \tilde{F}_d e^{i\omega t} \tag{10}$$

the response amplitude $\tilde{y}_n(x)$ can be obtained from Eqs. (6)-(9) as

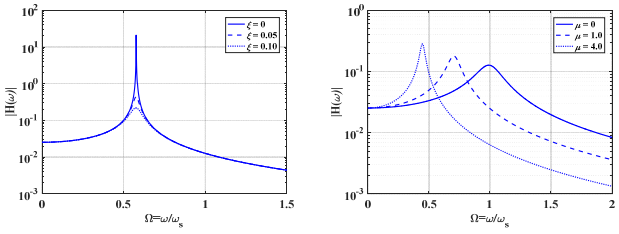

(a) For several ξ with $\mu = 2.0$ (b) For several μ with $\xi = 0.08$

Fig. 4 FRF curves for an ordinary SDOF system with a VIMD

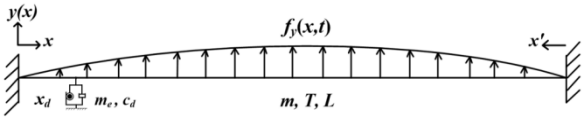

Fig. 5 A taut cable with a VIMD

$$\tilde{y}_n(x)=\begin{cases}\tilde{y}_n(x_d)\dfrac{sin(\beta x)}{sin(\beta x_d)}+\dfrac{\tilde{f}_nL^2}{T(n^2\pi^2-L^2\beta^2)}\left[\dfrac{sin(\beta x)}{sin(\beta x_d)}sin\left(\dfrac{n\pi x_d}{L}\right)-sin\left(\dfrac{n\pi x}{L}\right)\right], \\ (0<x<x_d) \\ \tilde{y}_n(x'_d)\dfrac{sin(\beta x')}{sin(\beta x'_d)}+\dfrac{\tilde{f}_nL^2}{T(n^2\pi^2-L^2\beta^2)}\left[\dfrac{sin(\beta x')}{sin(\beta x'_d)}sin\left(\dfrac{n\pi x'_d}{L}\right)-sin\left(\dfrac{n\pi x'}{L}\right)\right], \\ (0<x'<x'_d)\end{cases} \tag{11}$$

where β is the wavenumber, which is proportional to the frequency of excitation ω

$$\beta=\omega\sqrt{\frac{m}{T}} \tag{12}$$

The longer cable segment ($0<x'<x'_d$) will be our main focus for investigation in this study, since the distance x_d to the VIMD from an end is usually small, set to 0.02 L (unless explicitly stated). By substituting Eq. (11) into Eq. (9), the amplitude $\tilde{y}_n(x_d)$ at x_d can be obtained in terms of the external force and damper parameters

$$\tilde{y}_n(x_d)=\frac{\tilde{f}_nL}{(n^2\pi^2-L^2\beta^2)}\frac{n\pi(1+(-1)^n)cos\left(\frac{n\pi x_d}{L}\right)-\beta Lsin\left(\frac{n\pi x_d}{L}\right)[cot(\beta x_d)+(-1)^{n+1}cot(\beta x'_d)]}{-\beta^2T\frac{m_e}{m}+ic_d\beta\sqrt{\frac{T}{m}}+\beta T[cot(\beta x_d)+cot(\beta x'_d)]} \tag{13}$$

Substituting Eq. (13) into Eq. (11) gives $\tilde{y}_n(x')$ at x' for $0<x'<x'_d$

$$\begin{aligned}\tilde{y}_n(x')=&\frac{\tilde{f}_nL}{(n^2\pi^2-L^2\beta^2)}\frac{n\pi(1+(-1)^n)cos\left(\frac{n\pi x_d}{L}\right)-\beta Lsin\left(\frac{n\pi x_d}{L}\right)[cot(\beta x_d)+(-1)^{n+1}cot(\beta x'_d)]}{-\beta^2T\frac{m_e}{m}+ic_d\beta\sqrt{\frac{T}{m}}+\beta T[cot(\beta x_d)+cot(\beta x'_d)]}\frac{sin(\beta x')}{sin(\beta x'_d)}\\&+\frac{\tilde{f}_nL^2}{T(n^2\pi^2-L^2\beta^2)}\left[\frac{sin(\beta x')}{sin(\beta x'_d)}sin\left(\frac{n\pi x'_d}{L}\right)-sin\left(\frac{n\pi x'}{L}\right)\right]\end{aligned} \tag{14}$$

Subsequently, the FRF $H_n(\beta,\,x')$ for $y(x')$ at x' can be obtained in terms of the wavenumber and damper parameters

$$\begin{aligned}H_n(\beta,\,x')=&\frac{Lsin(\beta x')}{(n^2\pi^2-L^2\beta^2)sin(\beta x'_d)sin\left(\frac{n\pi x'}{L}\right)}\frac{n\pi(1+(-1)^n)cos\left(\frac{n\pi x_d}{L}\right)-\beta Lsin\left(\frac{n\pi x_d}{L}\right)\begin{bmatrix}cot(\beta x_d)\\+(-1)^{n+1}cot(\beta x'_d)\end{bmatrix}}{-\beta^2T\frac{m_e}{m}+ic_d\beta\sqrt{\frac{T}{m}}+\beta T[cot(\beta x_d)+cot(\beta x'_d)]}\\&+\frac{L^2}{T(n^2\pi^2-L^2\beta^2)}\left[\frac{sin(\beta x')sin\left(\frac{n\pi x'_d}{L}\right)}{sin(\beta x'_d)sin\left(\frac{n\pi x'}{L}\right)}-1\right]\end{aligned} \tag{15}$$

For the peak values of $H_n(\beta,\,x')$ in Eq. (15), the denominators may become 0 in three cases, specifically: Case (*i*) $\frac{n\pi x'}{L}=k\pi$; Case (*ii*) $\beta=\frac{n\pi}{L}$; and Case (*iii*) $\beta x'_d=j\pi$, where k and j are natural numbers ($k\le n$). Case (*i*) can be disregarded, because it means that the response point x' is at the nodal point of the excited mode. Case (*ii*) indicates a resonant vibration for the original undamped nth mode. Case (*iii*) means that the excitation frequency is j times the first natural frequency of the first natural frequency of the longer cable segment ($0<x'<x'_d$). This case can be approximately considered as $\beta=\frac{j\pi}{L}$ as in Case (*ii*), because x_d is very small and $x'_d\approx L$. The peak value of $H_n(\beta,\,x')$ at $\beta=\frac{n\pi}{L}$ can be evaluated using L'Hospital's rule, as in Eq. (16).

$$\begin{aligned}H_n(\beta,\,x')=&\frac{(-1)^{n+1}L^2}{2n^2\pi^2sin\left(\frac{n\pi x_d}{L}\right)}\frac{\begin{matrix}-L\left[cos\left(\frac{n\pi x_d}{L}\right)-cot\left(\frac{n\pi x_d}{L}\right)sin\left(\frac{n\pi x'_d}{L}\right)\right]\\+n\pi\left[x_dcsc\left(\frac{n\pi x_d}{L}\right)+x'_dcsc^2\left(\frac{n\pi x_d}{L}\right)sin\left(\frac{n\pi x'_d}{L}\right)\right]\end{matrix}}{n\pi T\frac{m_e}{m}-ic_dL\sqrt{\frac{T}{m}}}\\&+(-1)^{n+1}L\frac{(-1)^nx'_dcot\left(\frac{n\pi x_d}{L}\right)-x'cot\left(\frac{n\pi x'}{L}\right)csc\left(\frac{n\pi x_d}{L}\right)sin\left(\frac{n\pi x'_d}{L}\right)}{2n\pi T},\qquad \beta=\frac{n\pi}{L},\ n=1,2,3,\ldots\end{aligned} \tag{16}$$

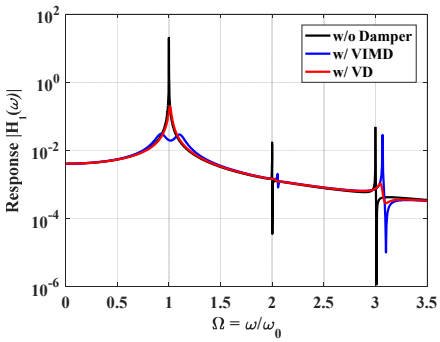

Fig. 6 FRF curves $H_1(\omega)$ of a cable at $x_r' = 0.5\,L$ with various dampers

Fig. 6 gives the FRF curves $H_1(\omega, x')$ of a taut cable with various dampers for a distributed load proportional to the first mode. The response point is at $x_r' = 0.5\,L$. The VIMD has the optimal inertial mass (m_e) to control the first cable mode vibration. The related procedure will be discussed in Section 3. The horizontal axis is the frequency ratio ($\Omega = \omega/\omega_0$) with respect to the first natural frequency of the cable without a VIMD, $\omega_0 = \frac{\pi}{L}\sqrt{\frac{T}{m}}$. The vertical axis $H_1(\omega)$ in Eq. (15) is shown in the logarithmic scale. It can be seen that a conventional viscous damper (VD) causes the resonant response to decrease. The FRF curve with a VIMD controlling the first cable mode shows that the VIMD on a cable splits the target cable mode into two vibration modes and decreases the response amplitude, whereas the VIMD only causes the other natural frequencies to increase, as shown in Fig. 6. The mode split by a VIMD on a cable is a very interesting phenomenon and contrasts with the single decrement of the resonant frequency by a VIMD on an ordinary structure (see Fig. 4).

3. Optimal design of a VIMD on a cable

3.1 Revisit of fixed-points method for TMD design

A major aspect of structural control is to suppress the response around the natural resonant frequency. As we mentioned above, analyzing the frequency response curve is the basis of a traditional design method called, the fixed-points method (FPM), which was originally proposed by Den Hartog for the tuned mass damper (TMD). For an undamped SDOF system with a TMD (Fig. 7(a)), the frequency response function $H(\Omega)$ of the primary mass m_s can be obtained as

$$H(\Omega) = \sqrt{\frac{(2\xi_d\Omega f)^2 + (\Omega^2 - f^2)^2}{(2\xi_d\Omega f)^2(\Omega^2 - 1 + \mu\Omega^2)^2 + [\mu f^2\Omega^2 - (\Omega^2 - 1)(\Omega^2 - f^2)]^2}} \tag{17}$$

where μ is the mass ratio $\frac{m_d}{m_s}$; ξ_d is the damping ratio of the TMD $\frac{c}{2m_d\omega_s}$; f is the frequency ratio $\frac{\omega_d}{\omega_s}$; ω_d is the natural frequency of the TMD; and Ω is the excitation frequency ratio $\frac{\omega}{\omega_s}$.

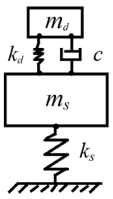

(a) An undamped SDOF system with a TMD

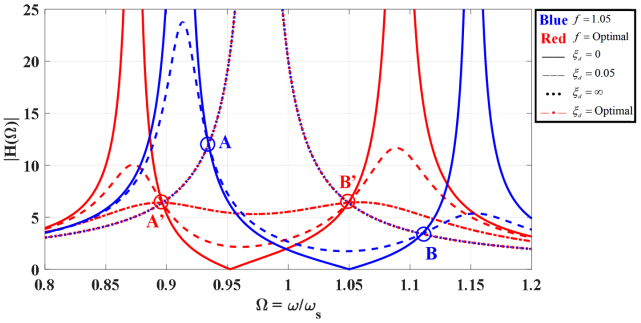

(b) FRF curves of m_s for various f and ξ with $\mu = 0.05$

Fig. 7 An undamped SDOF system with a TMD

Then, the optimal TMD parameters can be obtained for a given mass ratio μ as Den Hartog (1934)

$$f^{opt} = \frac{1}{1+\mu}, \qquad k_d^{opt} = \frac{\mu}{(1+\mu)^2}k_s, \qquad \xi_d^{opt} = \sqrt{\frac{3\mu}{8(1+\mu)^3}} \tag{18}$$

Fig. 7(b) shows the frequency response function (FRF) curves for various TMD parameters (f = 0.95 and f = 1.05; and ξ_d = 0, 0.05, and ∞), wherein the red dash-dot curve (—•—) represents the case with the optimal f and ξ_d of Eq. (18). FRF curves become infinite near the resonant frequency ω_s, when ξ_d is zero or infinite. This means that there is an optimal ξ_d between two values of 0 and ∞, which leads to the minimum peak response. It can be clearly observed that all FRF curves pass through 2 points (A and B or A' and B') with a selected f, regardless of the value of ξ_d. Therefore, the FRF responses at the two points need to be tuned as low as possible by selecting f (i.e., ω_d and k_d) before searching the optimal ξ_d. It can also be seen that two FRF curves with different f become the same, when ξ_d reaches infinity and constrains the relative motion between m_s and m_d. As f increases from 0.95 to 1.05, the fixed points (A' and B') move to the right (A and B) along the FRF curve with an infinite ξ_d, while the height of one fixed point goes up ($A' \to A$) and the other down ($B' \to B$). Hence the FRF curve with an infinite ξ_d curve may be used as a base curve in the optimal design of a TMD.

Based on the properties of the FRF curves with regard to

the various TMD parameters discussed above, the FPM for the optimal design of a TMD for the minimum structural response was developed in references (Den Hartog 1934, Brock 1946, Ren 2001, Krenk 2005, Ozer and Royston 2005), the procedures for which are summarized as:

Step 1 for the optimal f: The optimal TMD frequency ratio f (i.e., the k_d for a specified μ) is obtained to make the FRF values at two fixed points equal.

Step 2 for the optimal ξ_d: The optimal TMD damping ratio ξ_d is selected to make the FRF curve pass through the two points horizontally, so that the FRF may have the maximum value at the two fixed points (shown as a red dash-dot curve in Fig. 7(b)).

3.2 Optimal VIMD design for a cable with the fixed-points method

In this study we propose an optimal design procedure for a VIMD on a cable using the FPM similarly to a TMD design on an undamped SDOF system as discussed in Fig. 7 and Section 3.1. First, we investigated the characteristics of the FRF curve $H_1(\Omega)$ at $x_r' = 0.5\,L$ for several VIMD parameters ($\bar{m}_e$ and $\bar{c}_d$) shown in Fig. 8. Two cases of inertial mass ($\bar{m}_e$) were considered along with several values of the damping coefficient ($\bar{c}_d$). The VIMD parameters (m_e and c_d) were nondimensionalized as (Lu *et al*. 2017)

$$\bar{m}_e = \frac{m_e L\omega_0^2}{\pi^2 T} = \frac{m_e}{mL}, \qquad \bar{c}_d = \frac{c_d L\omega_0}{\pi^2 T} = \frac{c_d}{\sqrt{mT}}, \qquad \Omega = \frac{\omega}{\omega_0} \tag{19}$$

where ω_0 is the first natural frequency of the cable without a VIMD: $\omega_0 = \frac{\pi}{L}\sqrt{\frac{T}{m}}$.

It is evident that the general trends of the FRF curves in cable response to the VIMD parameters were very similar to those of the undamped SDOF system to the TMD parameters shown in Fig. 7. The first resonant frequency in $H_1(\Omega)$ split into two in each case of $\bar{m}_e$ with a small value of $\bar{c}_d$. All FRF curves passed through two points (A and B for $\bar{m}_e = 4.5$; or A' and B' for $\bar{m}_e = 5$), regardless of $\bar{c}_d$. In the case of $\bar{c}_d$ being zero, each FRF curves for different $\bar{m}_e$ values had two peaks with infinite amplitudes at the split frequencies. On the other hand, in the case of $\bar{c}_d$ being infinite, two FRF curves for different $\bar{m}_e$ became the same, producing one peak with infinite amplitude.

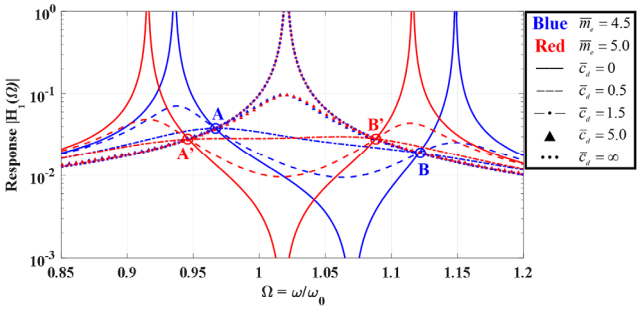

Fig. 8 FRF curves $H_1(\Omega)$ of a cable at $x_r' = 0.5\,L$ with various VIMD parameters

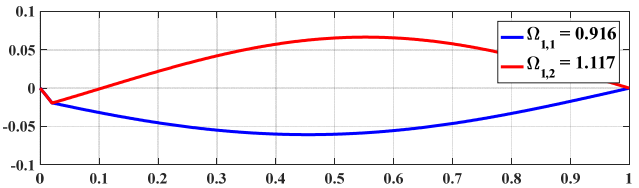

(a) Split mode shapes of the 1st original mode

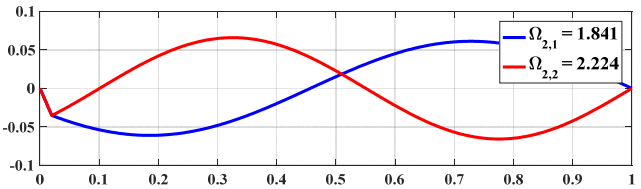

(b) Split mode shapes of the 2nd original mode

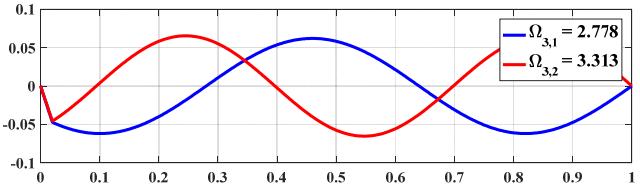

(c) Split mode shapes of the 3rd original mode

Fig. 9 Split mode shapes of three original modes ($\bar{c}_d = 0$)

Fig. 9(a) shows two cable mode shapes split from the first mode without a VIMD by simply introducing $\bar{m}_e$ optimized to the first mode. Figs. 9(b) and (c) show the split modes due to $\bar{m}_e$ optimized to the second and third modes, respectively. It is interesting to see that both split modes have slope discontinuity at the VIMD point (x_d) and two mode shapes are out of phase in the longer segment of the cable; while the split frequencies ($\Omega_{n,1}$ and $\Omega_{n,2}$) are fairly close, which may be the major mechanism for the VIMD to significantly reduce cable vibration.

3.3 Optimal inertial mass of a VIMD

First, the optimal inertial mass is obtained by making the amplitudes of $H_n(\beta,\ x')$ in Eq. (15) equal at two fixed points. The fixed points can be subsequently determined by the property of "independence of damping". Since the viscous damping force is proportional to the velocity, the damping term (c_d) represents the imaginary part of the FRF in Eq. (15), which can be simplified as

$$H_n = \frac{N_r + iN_i c_d}{D_r + iD_i c_d} \tag{20}$$

where N_r and $N_i c_d$ are the real and imaginary parts of the numerator, and D_r and $D_i c_d$ are those of the denominator. Independence of damping for two fixed points means that $|H_n|$ at two points is not affected by c_d, and can be mathematically achieved by

$$\left(\frac{N_r}{D_r}\right)^2 = \left(\frac{N_i}{D_i}\right)^2 \quad \Rightarrow \quad N_r D_i = \pm N_i D_r \tag{21}$$

Eq. (15) can also be rewritten as

$$H_n = \frac{A}{B + iCc_d} + D = \frac{A + BD + iCDc_d}{B + iCc_d} \tag{22}$$

where

$$\begin{aligned} A &= \frac{L\left[n\pi(1+(-1)^n)cos\left(\frac{n\pi x_d}{L}\right) - \beta L sin\left(\frac{n\pi x_d}{L}\right)[cot(\beta x_d) + (-1)^{n+1}cot(\beta x_d')]\right]}{(n^2\pi^2 - L^2\beta^2)sin(\beta x_d')sin\left(\frac{n\pi x'}{L}\right)} sin(\beta x') \\ B &= -\beta^2 T\frac{m_e}{m} + \beta T[cot(\beta x_d) + cot(\beta x_d')] \\ C &= \beta\sqrt{\frac{T}{m}} \\ D &= \frac{L^2}{T(n^2\pi^2 - L^2\beta^2)}\left[\frac{sin(\beta x')sin\left(\frac{n\pi x_d'}{L}\right)}{sin(\beta x_d')sin\left(\frac{n\pi x'}{L}\right)} - 1\right] \end{aligned} \tag{23}$$

From Eqs. (21) and (22) the following relation can be obtained

$$A + BD = \pm BD \tag{24}$$

For Eq. (24), two solutions exist. One is $A + BD = BD$, which yields $A = 0$

$$\frac{L\left[n\pi(1+(-1)^n)cos\left(\frac{n\pi}{L}x_d\right) - \beta L sin\left(\frac{n\pi x_d}{L}\right)[cot(\beta x_d) + (-1)^{n+1}cot(\beta x_d')]\right]}{(n^2\pi^2 - L^2\beta^2)sin(\beta x_d')sin\left(\frac{n\pi x'}{L}\right)} sin(\beta x') = 0 \tag{25}$$

The solutions of Eq. (25) for the nth target cable mode only depend on the damper location ($sin\left(\frac{n\pi x_d}{L}\right) = 0$, which means that the VIMD is set at the nodal point of the nth mode), and the response point ($sin(\beta x') = 0$, which means that the response point is the nodal point of the nth mode). It can be also found that the first term in Eq. (15) which contains the VIMD parameters becomes zero when $A = 0$. This means that the fixed points obtained by Eq. (25) are not determined by the VIMD parameters. Therefore, the solutions of Eq. (25) are not interesting to consider.

The other case is $A + 2BD = 0$, which can be expressed as

$$\beta\frac{m_e}{m} = \frac{n\pi(1+(-1)^n)\cos\left(\frac{n\pi}{L}x_d\right)\sin(\beta x')}{2\beta L\left[\sin(\beta x')\sin\left(\frac{n\pi x_d'}{L}\right) - \sin(\beta x_d')\sin\left(\frac{n\pi x'}{L}\right)\right] + [\cot(\beta x_d) + \cot(\beta x_d')]} - \frac{\sin\left(\frac{n\pi x_d}{L}\right)[\cot(\beta x_d) + (-1)^{n+1}\cot(\beta x_d')]\sin(\beta x')}{2\left[\sin(\beta x')\sin\left(\frac{n\pi x_d'}{L}\right) - \sin(\beta x_d')\sin\left(\frac{n\pi x'}{L}\right)\right]} \tag{26}$$

Eq. (26) can be solved for β from the intersections of the linear function of β on the left hand side of the equation, and the transcendental function of β on the right hand side. For the nth target cable mode, there are two intersections (β_A and β_B) near the nth natural frequency ($\beta = \frac{n\pi}{L}$), as shown in Fig. 10. Two points (β_A and β_B) depend on the value of m_e, which can be obtained from the condition of equal amplitude

$$H_n(\beta_A(m_e), \quad x') = H_n(\beta_B(m_e), x') \tag{27}$$

Eq. (27) is solved for m_e, β_A, and β_B by taking $c_d = 0$, considering the independence of c_d at the two fixed points on the FRF curve as well as the computational efficiency, using the *fslove* function in Matlab. The initial values of β_A and β_B are taken as $\frac{n\pi}{L}$ and $\frac{n\pi}{x_d'}$, respectively, with $n = 1,2,3,\ldots$, based on the following discussion.

The inertial mass is essentially a large mass when the cable vibrates as shown in Fig. 11(a). Therefore, the VIMD can be simplified as in Fig. 11(b), where $k_g = T\left(\frac{1}{x_d} + \frac{1}{x_d'}\right)$ is the geometric stiffness from two cable segments (with x_d and x_d') with initial tension T. By neglecting the cable mass, the equation of motion of the inertial mass can be approximated as

$$m_e\ddot{y}_d + c_d\dot{y}_d + T\left(\frac{1}{x_d} + \frac{1}{x_d'}\right)y_d = 0 \tag{28}$$

The corresponding natural frequency ω_{VIMD} can be obtained as

$$\omega_{VIMD}^2 = \frac{TL}{m_e x_d x_d'} \tag{29}$$

If ω_{VIMD} is tuned close to the natural frequency of the target mode, m_e can be obtained from Eqs. (19) and (29)

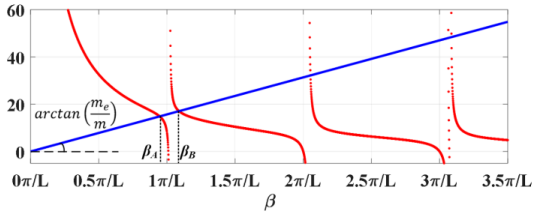

(a) β_A and β_B for $n = 1$ and $x_r' = 0.5\,L$

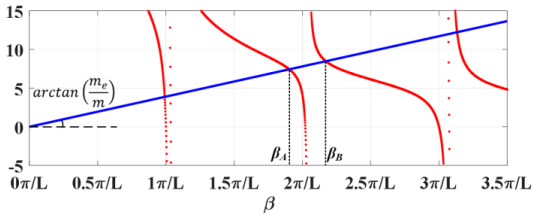

(b) β_A and β_B for $n = 2$ and $x_r' = 0.25\,L$

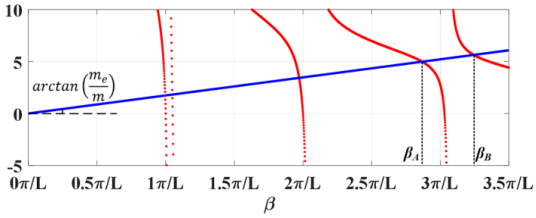

(c) β_A and β_B for $n = 3$ and $x_r' = 0.5\,L$

Fig. 10 Solutions of Eq. (26) for β_A and β_B (—: linear function on the left, ⋯: transcendental function on the right)

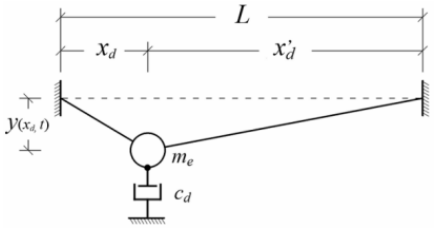

(a) Taut cable with large mass and damping

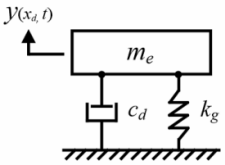

(b) Simplified VIMD model

Fig. 11 Simplified VIMD model

$$m_{e,initial} = \frac{1}{n^2}\frac{mL^3}{\pi^2 x_d x_d'}, \qquad n = 1,2,3,\ldots \tag{30}$$

Eq. (30) can be effectively used as an initial value of m_e for solving Eq. (27).

The optimal VIMD mass ($\bar{m}_e$) and frequencies at two fixed points (β_A and β_B) are shown for the first 3 control modes in Table 1. The values of β_A and β_B are about 6~7% off from the wavenumber of each locked cable mode $\frac{n\pi}{x_d'}$, when $x_d = 0.02\,L$. It is interesting to observe that the

Table 1 Dimensionless optimal $\bar{m}_e$ for the first 3 modes

	1st mode	2nd mode	3rd mode
Response point x_r'	$L/2$	$L/4$	$L/2$
$\bar{m}_e$	4.988	1.243	0.553
β_A	$\frac{0.9471\pi}{L}$	$\frac{1.9179\pi}{L}$	$\frac{2.8685\pi}{L}$
β_B	$\frac{1.0888\pi}{L}$	$\frac{2.1823\pi}{L}$	$\frac{3.2439\pi}{L}$

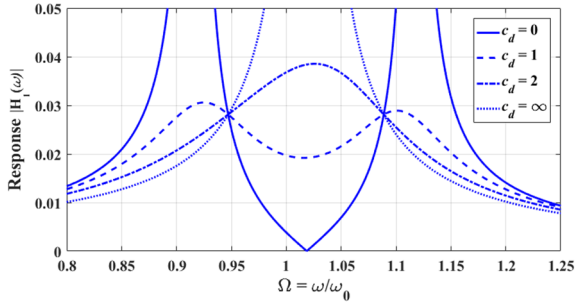

(a) With optimal $\bar{m}_e$ for the 1st mode

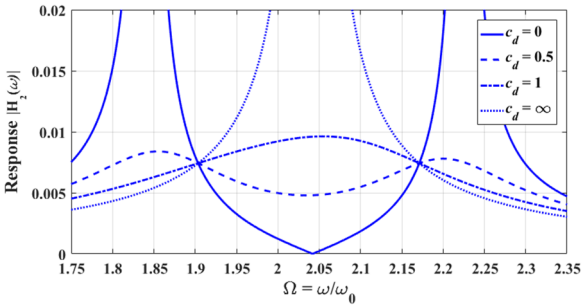

(b) With optimal $\bar{m}_e$ for the 2nd mode

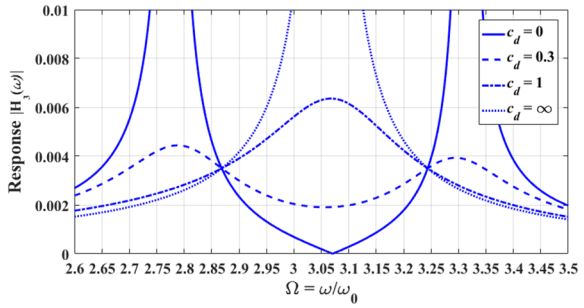

(c) With optimal $\bar{m}_e$ for the 3rd mode

Fig. 12 FRF curves with optimal $\bar{m}_e$ and various $\bar{c}_d$ for the first 3 modes

optimal mass $\bar{m}_e$ is inversely proportional to the squares of the mode number n in approximation, which is proportional to the natural frequency; i.e., $4.99 : 1.24 : 0.55 \approx \frac{1}{1} : \frac{1}{4} : \frac{1}{9}$, as indicated by Eq. (30).

The FRF curves with the optimal $\bar{m}_e$ for the first 3 modes are shown for various $\bar{c}_d$ in Fig. 12. The response point x_r' is $0.5\,L$ for the 1st and 3rd mode and $0.25\,L$ for the 2nd mode. Each of the original cable modes split into two with the introduction of $\bar{m}_e$. As expected, the FRFs related to both split modes became closer with increasing

Table 2 Dimensionless optimal damping coefficients for the first 8 modes

Target modes	$\bar{m}_e$	at β_A and β_B		Mean $\bar{c}_d$		Reference parameters (Lu *et al*. 2017)			
		Ω_n	$\bar{c}_d$	$\bar{c}_d$	ξ_n	$\bar{m}_e$	$\bar{c}_d$	Ω_n	ξ_n
1.	4.988	0.949	1.352	1.275	6.83%	4.808	2	1.003	9.76%
		1.089	1.198		5.43%			1.039	9.88%
2.	1.243	1.918	0.720	0.679	6.65%	1.198	1.05	2.011	9.37%
		2.182	0.638		5.28%			2.073	9.49%
3.	0.553	2.869	0.518	0.484	6.25%	0.529	0.75	3.026	8.79%
		3.244	0.449		4.80%			3.103	9.05%
4.	0.309	3.854	0.438	0.409	5.78%	0.295	0.61	4.048	8.28%
		4.305	0.379		4.64%			4.124	8.51%
5.	0.199	4.840	0.388	0.354	5.30%	0.187	0.53	5.065	7.71%
		5.356	0.319		4.00%			5.152	8.03%
6.	0.136	5.848	0.368	0.335	4.98%	0.128	0.48	6.061	7.20%
		6.399	0.301		3.82%			6.201	7.47%
7.	0.101	6.847	0.353	0.312	4.53%	0.092	0.45	7.082	6.84%
		7.437	0.271		3.28%			7.222	7.00%
8.	0.076	7.867	0.346	0.307	4.26%	0.069	0.42	8.107	6.63%
		8.471	0.267		3.13%			8.234	6.49%

$\bar{c}_d$, and became a locked mode when $\bar{c}_d$ approached infinity. The amplitudes of the FRF at two fixed points were tuned to be equal to each other by selecting the optimal $\bar{m}_e$.

3.4 Optimal viscous damping of a VIMD

The optimal damping coefficient is obtained by making the FRF curve reach maximum value at both points. Therefore, the slope shall be zero at two points

$$\left.\frac{\partial|H_n(\beta,\ c_d)|}{\partial\beta}\right|_{\beta_A,\,\beta_B} = 0 \tag{31}$$

Obviously, Eq. (31) can-not be satisfied simultaneously at both points with only one value of c_d. Hence, the damping coefficient is evaluated at each point, and the mean value is taken as the optimal value. The optimal parameters of the first eight modes are shown in Table 2. The last column shows the VIMD parameters obtained for the maximum modal damping ratios for the two split modes as the reference values for comparison; we obtained those using the state-space method (Lu *et al*. 2017). One can see that the required $\bar{c}_d$ values for β_A of each mode were slightly larger than those for β_B, and the modal damping ratio ξ_n of the lower split frequency was higher than that of the higher split frequency. The values of optimal $\bar{m}_e$ for each mode were similar with both methods. The optimal $\bar{c}_d$ using the fixed-point method was 25-35% lower than that obtained by the reference method, and so was the corresponding ξ_n. Moreover, with the reference parameters the frequencies and ξ_n of the two split modes were almost the same and the split frequencies were close to the original natural frequencies of the cable.

Fig. 13 shows the FRF curves resulting from different optimal VIMD parameters in the first three modes. We found that the FRF curves resulting from the mean values of $\bar{c}_d$ determined in the present study had nearly maximum values at the two fixed points. The FRF curves produced by the reference parameters (Lu *et al*. 2017) showed a single higher peak nearer the natural frequencies of the original

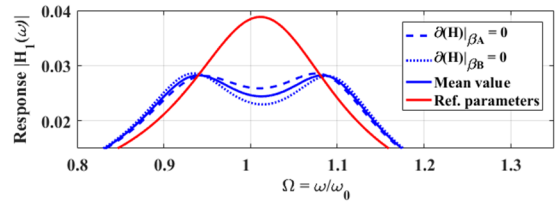

(a) With optimal $\bar{m}_e$ and $\bar{c}_d$ for the 1st mode

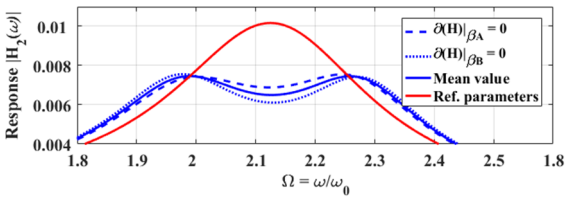

(b) With optimal $\bar{m}_e$ and $\bar{c}_d$ for the 2nd mode

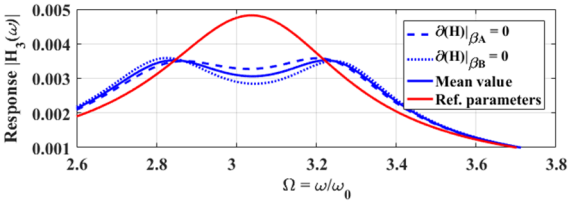

(c) With optimal $\bar{m}_e$ and $\bar{c}_d$ for the 3rd mode

Fig. 13 FRF curves of the first 3 modes using optimal VIMD parameters

cable than those produced by the present fixed-points method. The reduction of cable responses by manipulating two different optimal VIMD parameters will be discussed in the following section on simulation studies.

4. Numerical examples

In order to evaluate the performance of the proposed optimal VIMD parameters, we took the sectional properties of the cable from J26 cable on the 2nd Jiaojiang bridge (Zhejiang, China) for this simulation study (Table 3).

4.1 Concentrated harmonic load

As shown in Fig. 14, the concentrated harmonic load was set at $x_e = 0.98\,L$ and the damper at $x_d = 0.02\,L$. The envelope of load amplitude was taken as in Fig. 15(a), and the maximum amplitude was as $20\,kN$. The excitation frequencies were set as 0.488, 0.976, and $1.464\,Hz$, the same as the first 3 natural frequencies of the cable.

The cable-VIMD system has non-classical damping, hence we analyzed the responses with a state-space method using the *lsim* function in Matlab, and considered 50 modes with the shape function $\phi_n = sin(n\pi x)$. For the purpose of comparison, the responses were also obtained using the reference parameters in Table 2 and an optimal viscous damper (VD) obtained with Eq. (32) (Krenk 2000). The damper parameters are shown in Table 4.

$$\bar{c}_d = \frac{1}{\pi} csc\left(\frac{n\pi x_d}{L}\right) \tag{32}$$

Table 3 Cable parameters

Length	$L\,[m]$	255.4
Mass per unit length	$m\,[kg/m]$	100.8
Tension	$T\,[kN]$	6261
Diameter	$D\,[m]$	0.158
First 3 natural frequencies	$f_n[Hz]$	0.488, 0.976, and 1.464
Inherent modal damping ratio	ξ_d	0.2%

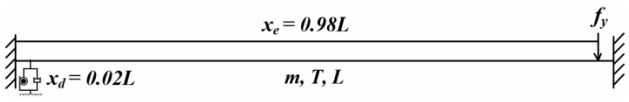

Fig. 14 A horizontal taut string cable with VIMD under a concentrated load

Table 4 Damper parameters for simulations

Target modes	Reference VD (Krenk 2000)	Reference VIMD (Lu *et al*. 2017)		Proposed optimal VIMD	
	c_d $[kNs/m]$	m_e $[ton]$	c_d $[kNs/m]$	m_e $[ton]$	c_d $[kNs/m]$
1.	400.1	123.8	157.9	128.4	100.6
2.	200.4	30.8	82.9	31.9	53.6
3.	134.1	13.6	59.2	14.2	38.2

The displacement histories were obtained at $x_r' = 0.5\,L$ for the 1st and 3rd modes and at $x_r = 0.25\,L$ for the 2nd mode. For the cable without dampers, the maximum responses due to excitation with the first two resonant frequencies were obtained as 2.6 m at $x_r = 0.5\,L$ and 1.3 m at $x_r = 0.75\,L$. The responses with dampers are shown in Figs. 15(b)-(d). Both of the optimal VIMDs (proposed and referenced) reduced cable vibration remarkably, i.e., to2-4% levels in the maximum responses without a damper, whereas the optimal VD reduced to a level of 13%.

Between the two VIMDs, the performance of the proposed VIMD was reduced to 35% levels of the referenced one. These results were expected in view of the FRF curves in Fig. 13.

4.2 Distributed random load

Performance of various dampers were investigated under a distributed random load. For calculation of the distributed load, the cable was divided into 20 segments with 19 nodes. 19 independent time histories were simulated for Gaussian white noise excitations with the same intensity and applied to the nodes. The average power spectral density of the excitations is shown in Fig. 16(a). A cable without a damper and three other cases with dampers optimized to the first mode were considered, as shown in Fig. 16.

Fig. 16(b) shows the root mean square (RMS) values of the displacement along the cable. Fig. 16(c) shows the displacement time histories at $x_r = 0.5\,L$. Figs. 16(d) and (e) show Fourier amplitude spectra (FAS) of the displacements at $x_r = 0.5\,L$ and $x_r = 0.75\,L$. It can be observed that both optimal VIMDs reduced the cable response very effectively, to 20-30% levels of the cable without a damper; whereas the VD reduced cable vibration to 50-60% levels. We found that the performance of the proposed optimal VIMD parameters was slightly better than that of the reference VIMD. The RMS displacement along the cable and the maximum displacement at $x_r = 0.5\,L$ using the presented VIMD are reduced to 89.2% and 91.2% levels of those using the reference VIMD. It is worth noting from Fig. 16(f) that the cable displacement at x_d by the present VIMD was the largest among three cases with a damper, which means the energy dissipation was enhanced due to the large damper travel. The damper force-displacement hysteresis seen in Fig. 16(f) indicates the negative stiffness effect of the VIMDs.

4.3 Earthquake load

To test the performance of the VIMDs under the earthquake load, EL Centro Earthquake as shown in Fig. 17(a) was considered. Figs. 17(b) and (c) show the RMS values of the displacement along the cable and the displacement time histories at $x_r = 0.5\,L$. Compared with the response without VIMD, the RMS displacement and the maximum displacement at $x_r = 0.5\,L$ are significantly reduced to 25-28% levels and to 38-51% levels by both of the optimal VIMDs, respectively. The performance of the proposed optimal VIMD parameters was slightly better than that of the reference VIMD. Fig. 17(d) shows the

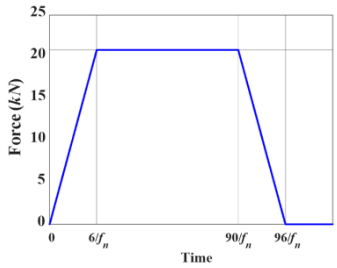

(a) Load envelope

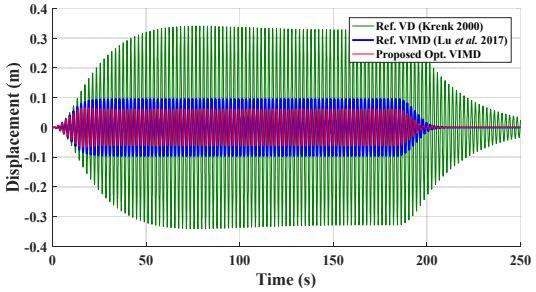

(b) Response at $x_r = 0.5\,L$ with a VIMD optimized to 1st mode (0.488 Hz)

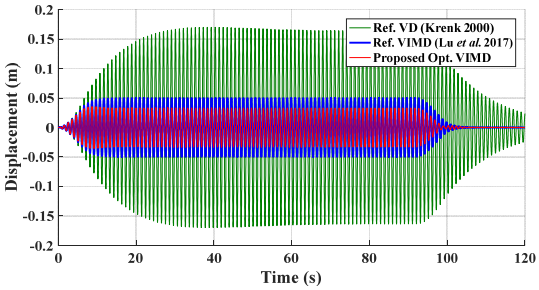

(c) Response at $x_r = 0.75\,L$ with a VIMD optimized to 2nd mode (0.976 Hz)

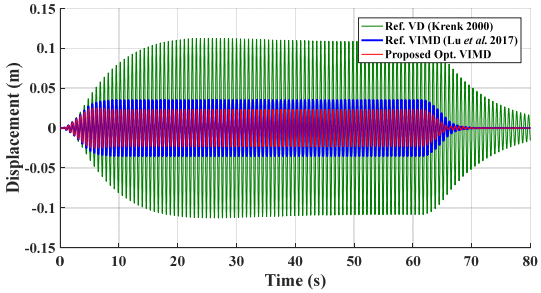

(d) Response at $x_r = 0.5\,L$ with a VIMD optimized to 3rd mode (1.464 Hz)

Fig. 15 Cable responses under a concentrated load with resonant frequencies

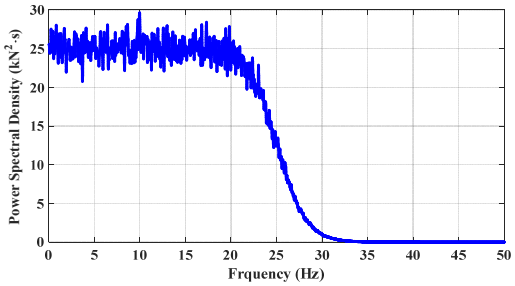

(a) Average PSD of the excitations

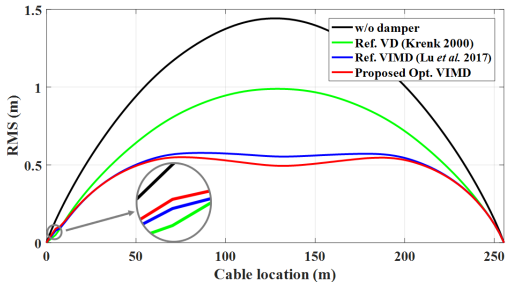

(b) RMS values of the displacement

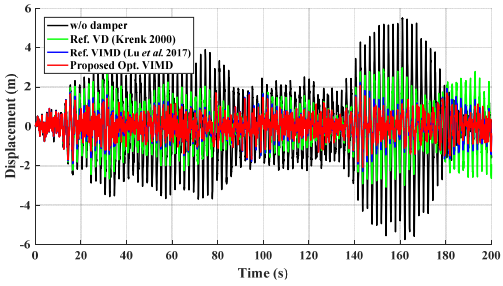

(c) Displacement time histories at $x_r = 0.5\,L$

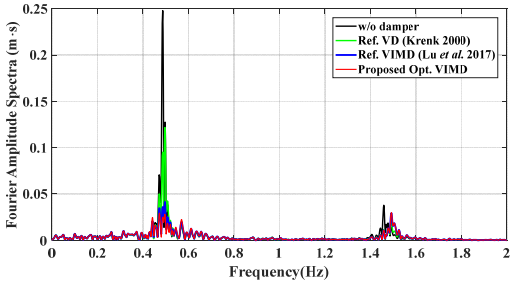

(d) FAS of the displacement at $x_r = 0.5\,L$

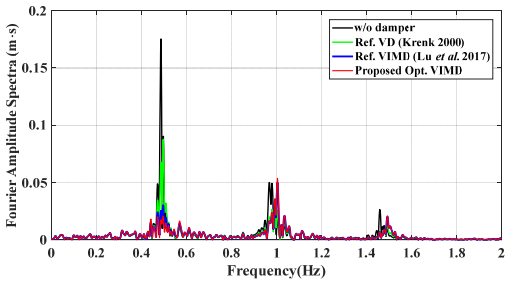

(e) FAS of the displacement at $x_r = 0.75\,L$

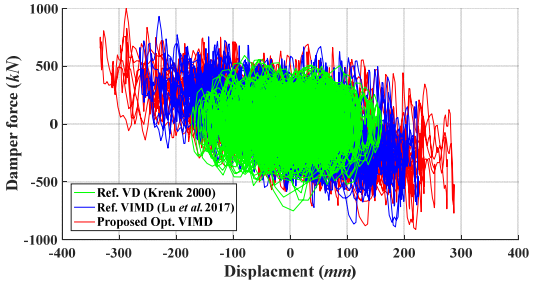

(f) Damper force-displacement hysteresis

Fig. 16 Cable responses with dampers optimized to 1st mode under a distributed random load

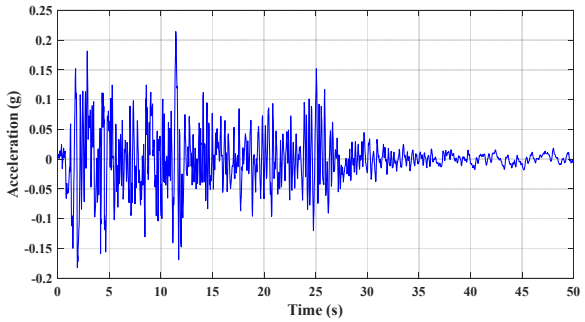

(a) EL Centro Earthquake

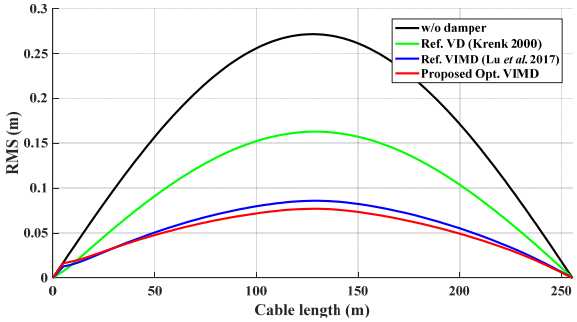

(b) RMS values of the displacement

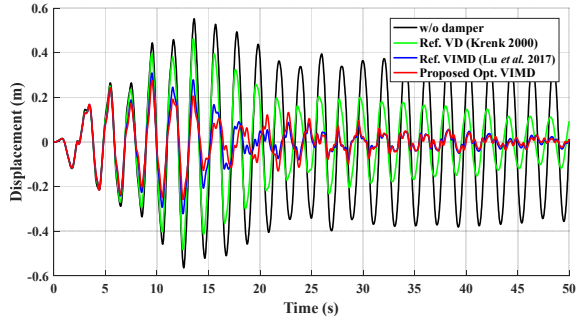

(c) Displacement time histories at $x_r = 0.5\,L$

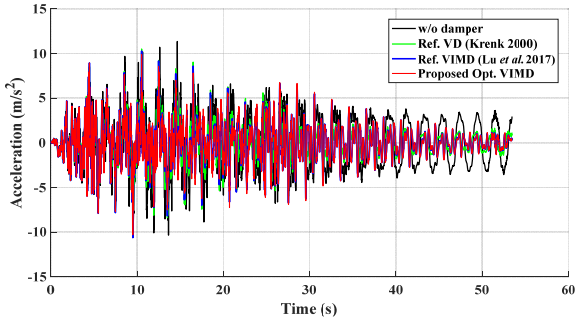

(d) Acceleration time histories at $x_r = 0.5\,L$

Fig. 17 Cable responses with dampers optimized to 1st mode under the EL Centro Earthquake

Table 5 Wind field simulation parameters

Simulation points n	19
Dividing frequency number N	2^{13}
Drag coefficient C_D	1.0
Upper cutoff frequency ω_{up} $[rad/s]$	20π
Frequency interval $\Delta\omega$ $[rad/s]$	0.0077
Time interval Δt $[s]$	0.05
Air density ρ $[kg/m^3]$	1.25
Coherence reduction coefficient λ	10

acceleration time histories at $x_r = 0.5\,L$. We observed that both of the time histories using the optimal VIMDs are similar, whereas their maximum amplitudes reduce to the level of 22.1% and 36.4% of those using the VD, respectively.

4.4 Random wind load

To test the performance of the VIMDs under wind load, we simulated 20 sets of random wind loads using 19 time histories for wind velocities at 19 nodes with an equal interval along the cable. The fluctuating wind velocities were simulated with Davenport's spectrum, taking into account the spatial coherence (Deodatis 1996, Cao *et al.* 2000, Duan *et al.* 2019a, b, c). Based on the Chinese Wind-resistant Design Specification for Highway Bridges, the mean wind velocity over 10 minutes at a height of 10 m was assumed to be $U_{10} = 60\frac{m}{s}$. The cable height (h) was assumed to be $30\,m$, and the corresponding hourly wind velocity at each node was then taken as $\bar{U}_{30} = 61.8\,m/s$ in order for the wind spectrum to simulate the fluctuating components of wind (Simiu and Scanlan 1996). The related parameters are given in Table 5.

Fig. 18 shows the time history of fluctuating velocity $u(x',t)$ of one set and its power spectral density (PSD) at $x' = 0.5\,L$ and $0.4\,L$, respectively. The PSDs of the simulated wind velocities at 2 locations were found to be well matched with the target PSD. Subsequently, the wind force was estimated approximately as

$$F_w \approx \frac{1}{2}\rho D\Delta L C_D U_{30}^2 + \rho D\Delta L C_D U_{30} u(x',t) \qquad (33)$$

where ρ, D, ΔL and C_D denote air density, cable diameter, cable segment length, and drag coefficient, respectively. U_{30} is the 10 minute wind velocity at $30\,m$ above the ground $(76.6\,m/s)$. The second term is the fluctuating component which was used for the dynamic response of the cable.

Figs. 19(a) and (b) give the cable displacements and FAS without a damper at the points where $x_r = 0.5\,L$ and $0.25\,L$, and show that the cable vibrated dominantly by the first mode under the wind load. The maximum responses were found to be $1.83\,m$ and $1.34\,m$ at these two locations. Therefore, we utilized the VIMD parameters optimized to the first mode.

Fig. 20 shows the responses with two optimal VIMDs. Figs. 20(a) and (b) represent for the FAS responses of one set of wind load at $x_r = 0.5\,L$ and $0.75\,L$, respectively. We found that the response at the first natural frequency was reduced remarkably by either of the optimal VIMDs compared with the response without a damper shown in Fig.

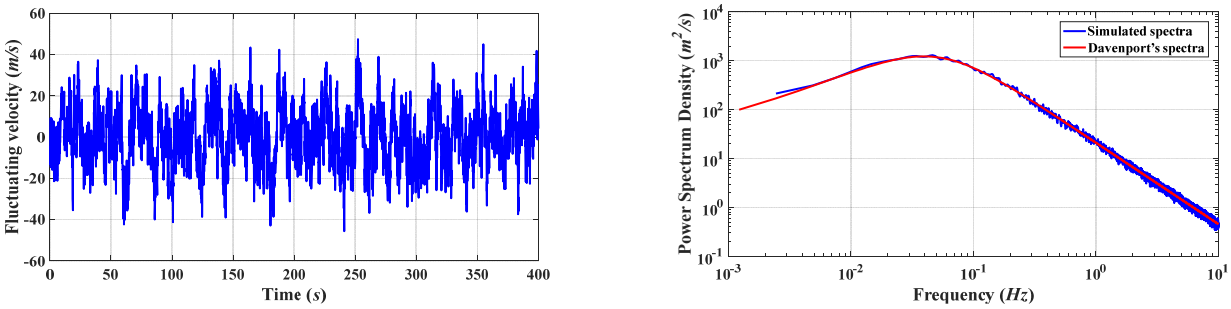

(a) Fluctuating velocity and power spectra at $x' = 0.5\,L$ and $h = 30\,m$

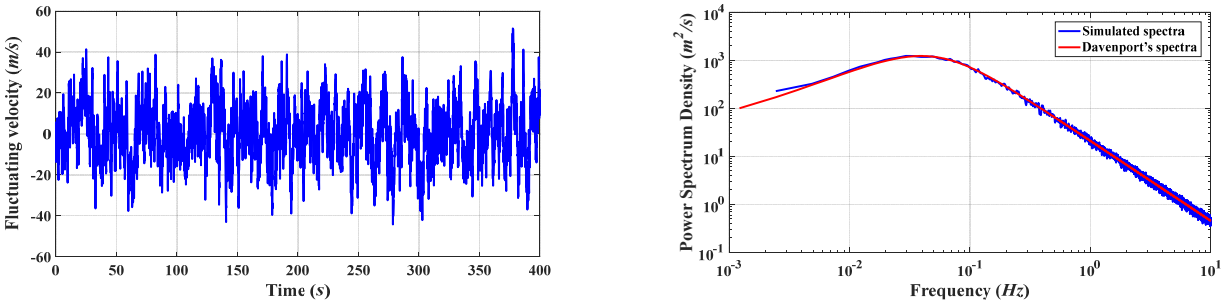

(b) Fluctuating velocity and power spectra at $x' = 0.4\,L$ and $h = 30\,m$

Fig. 18 Wind field simulation: $U_{10} = 60\,m/s$

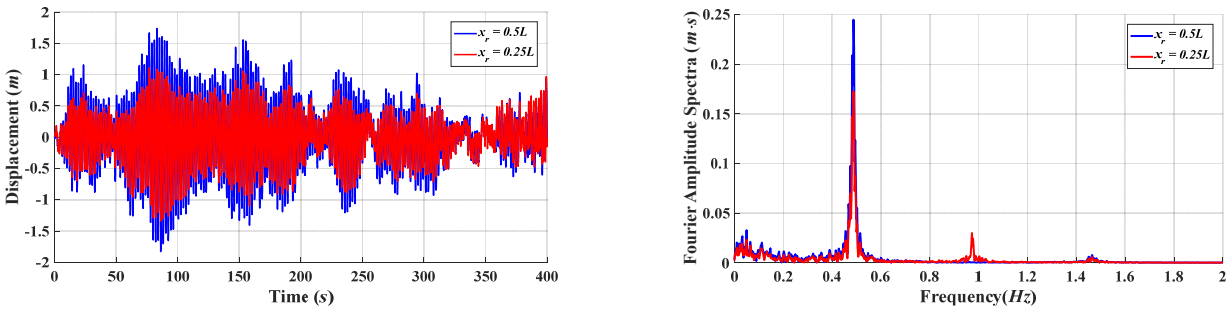

(a) Displacements at $x_r = 0.5\,L$ and $0.25\,L$ (b) FAS of the displacements at $x_r = 0.5\,L$ and $0.25\,L$

Fig. 19 Fluctuating components of wind responses without a damper

19(b). Fig. 20(c) shows the corresponding displacement time histories at $x_r = 0.5\,L$, which exhibited excellent vibration reduction by both VIMDs. The maximum responses are reduced to 25% levels of that without a damper. Fig. 20(d) shows the damper force-displacement hystereses using two optimal VIMDs and a conventional VD, proving the beneficial effect of the negative stiffness characteristics of the VIMD. Figs. 20(e) and (f) show the average RMS values of the displacement and the acceleration along the cable for 20 sets of wind loads. The present optimal VIMD gives slightly better performance over the reference one (at 95% levels in displacement and similar levels in acceleration).

4.5 Multiple VIMDs for multi-modes control

Especially for super long cables, cable vibrations with the higher cable modes often bring problems in the daily and maintenance operations of cable supported structures, which may be caused by the rain droplet or rivulet under the wind-rain condition or parametric excitations. Two cases of multiple VIMDs are considered for vibration reduction of the high frequency modes, and a 578 m-long cable of Sutong bridge is used as an example in this section, the cable parameters are shown in Table 6.

The VIMD layouts are: (*i*) 3 VIMDs with the 2nd and 3rd VIMDs added at 0.98L and 0.06L as in Fig. 21. The additional two VIMDs are optimized to the 2nd and 5th mode, and (*ii*) 3 VIMDs are respectively placed at 0.02 L,

Table 6 Parameters of a super long stay-cable

Length	$L\,[m]$	578.34
Mass per unit length	$m\,[kg/m]$	100.29
Tension	$T\,[kN]$	5471
Diameter	$D\,[m]$	0.124
First 3 natural frequencies	$f_n[Hz]$	0.202, 0.404, and 0.606
Inherent modal damping ratio	ξ_d	0.2%

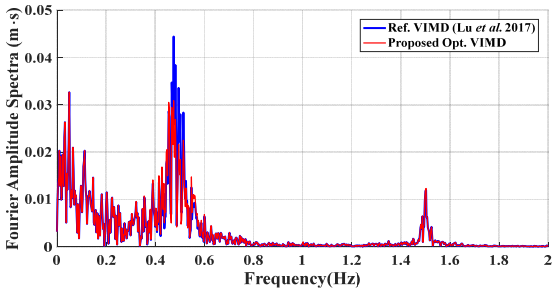

(a) FAS of the displacement at $x_r = 0.5\,L$

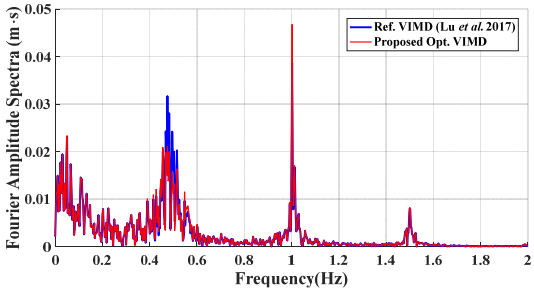

(b) FAS of the displacement at $x_r = 0.75\,L$

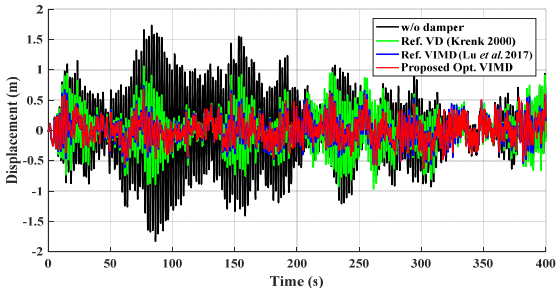

(c) Displacement time histories at $x_r = 0.5\,L$

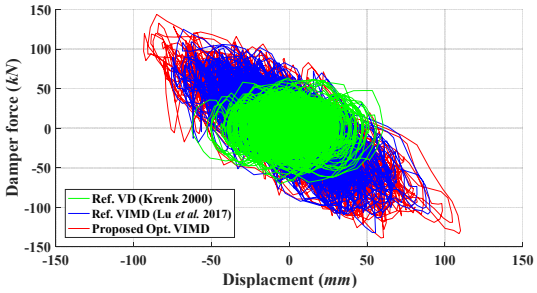

(d) Damper force-displacement hysteresis

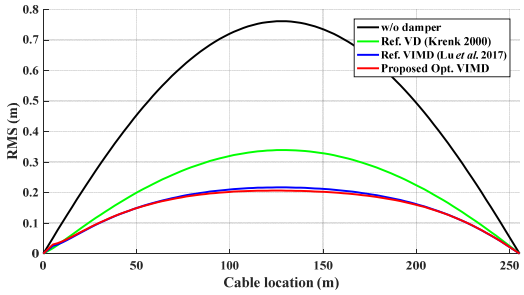

(e) Average RMS values of the displacement

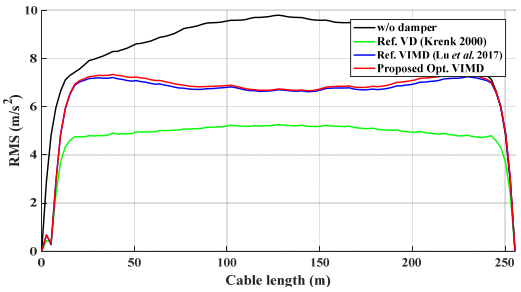

(f) Average RMS values of the acceleration

Fig. 20 Vibration results of the cable with a different damper under the fluctuating wind components (Red curves: the proposed optimal VIMD and Blue curves: the reference VIMD)

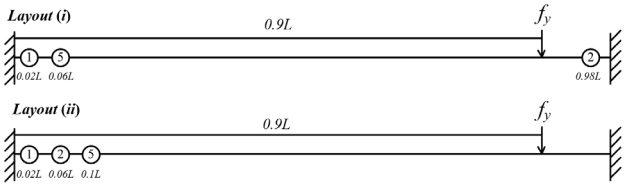

Fig. 21 Deployment of Multiple VIMDs

Table 7 Damper parameters for multiple VIMDs simulations

Layout (*i*)			Layout (*ii*)		
VIMD	$m_e[ton]$	$c_d[kNs/m]$	VIMD	$m_e[ton]$	$c_d[kNs/m]$
1.	289.3	93.8	1.	289.3	93.8
2.	72.1	50	2.	22.4	33.4
3.	1.99	20.6	3.	0.89	25.7

0.06 L, and 0.1 L, which are correspondingly optimized to the 1st, 2nd, and 5th mode. The VIMD parameters are shown in Table 7, where m_e decreases as the distance of the VIMD (x_d) from the cable end increases.

Table 8 Modal damping ratios using multiple VIMDs

Layout (*i*)			Layout (*ii*)		
Cable modes [*Hz*]		ξ_n	Cable modes [*Hz*]		ξ_n
1.	0.189	9.68%	1.	0.189	20.24%
2.	0.22	6.41%	2.	0.221	4.16%
3.	0.385	7.41%	3.	0.428	6.72%
4.	0.452	5.5%	4.	0.518	23.04%
5.	0.64	2.19%	5.	0.673	2.28%
6.	0.844	2.97%	6.	0.882	1.41%
7.	1.045	4.41%	7.	1.098	1.77%
8.	1.225	5.83%	8.	1.317	2.14%
9.	1.393	4.39%	9.	1.54	2.43%
10.	1.592	2.58%	10.	1.765	2.66%
11.	1.802	1.65%	11.	1.992	2.88%
12.	2.016	1.15%	12.	2.222	3.07%
13.	2.231	0.85%	13.	2.459	3.17%
14.	2.447	0.66%	14.	2.645	19.62%
15.	2.664	0.54 %	15.	2.701	2.95%

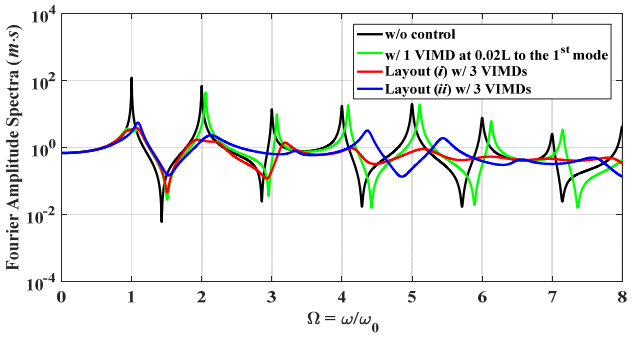

Fig. 22 FRF curves using multiple VIMDs at $x_r = 0.7\,L$

Table 8 shows the modal properties for two layouts. For Layout (*i*) with the 2nd VIMD for the 2nd mode placed well separately from the 1st one, the vibration modes get split at the first two target frequencies. However, the mode split of the 5th mode is not obvious due to the short distance from the 1st VIMD. For Layout (*ii*) with 3 closely placed VIMDs, the mode split is apparent only for the 1st target mode due to the interference between the VIMDs. The damping ratios with two VIMD layouts significantly increase even for the higher modes than the target modes, which are much larger than those obtained by Gao *et al*. (2019).

Fig. 22 shows the FRF curves at $x_r = 0.7\,L$ under a concentrated sinusoidal load at $x_e = 0.9\,L$ for several cases of the VIMD layout. The overall results in the splits of the target modes and increases of the modal damping ratios are found to be very similar to those in Table 8.

Then, a sinusoidal excitation with multi-components is considered with $f_y(t) = F_y sin(2\pi f_1 t) + 3F_y sin(2\pi f_2 t) + 6F_y sin(2\pi f_5 t)$, where $F_y = 20kN$ and $x_e = 0.9\,L$, as shown in Fig. 21. Fig. 23(a) shows the FAS of the displacements at $x_r = 0.7\,L$. As expected, both layouts using multiple VIMDs show good performances for reducing the response of higher modes, whereas using one single VIMD can only control one target mode. The

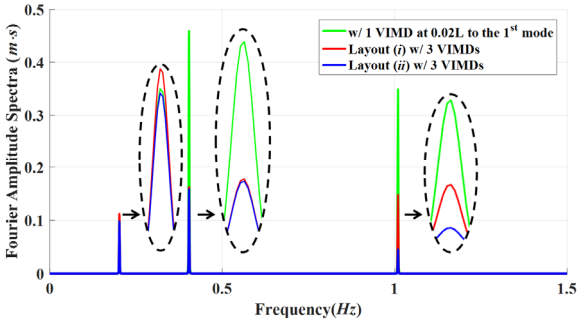

(a) FAS of the displacement at $x_r = 0.7\,L$

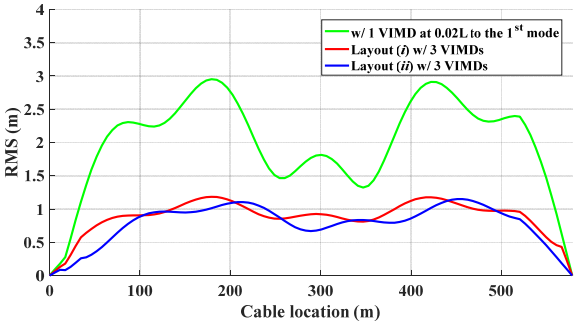

(b) RMS values of the displacement

Fig. 23 Cable response reduction by multiple VIMDs under sinusoidal excitation of multi-components

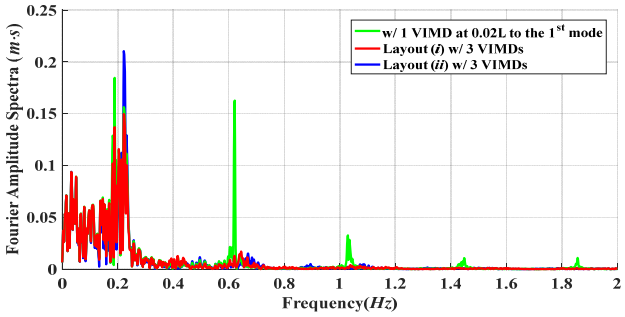

(a) FAS of the displacement at $x_r = 0.5\,L$

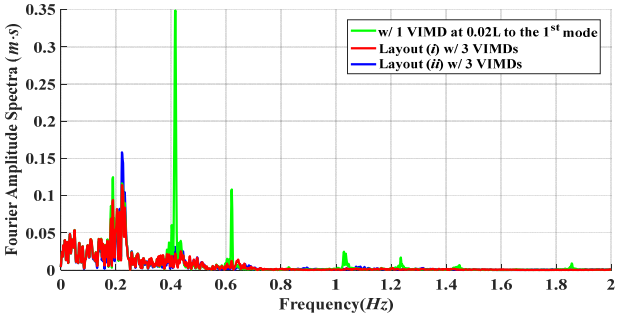

(b) FAS of the displacement at $x_r = 0.75\,L$

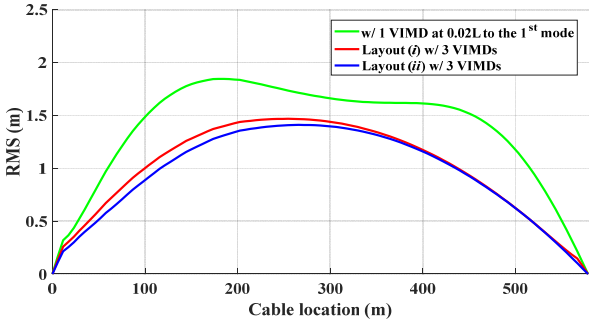

(c) RMS values of the displacement

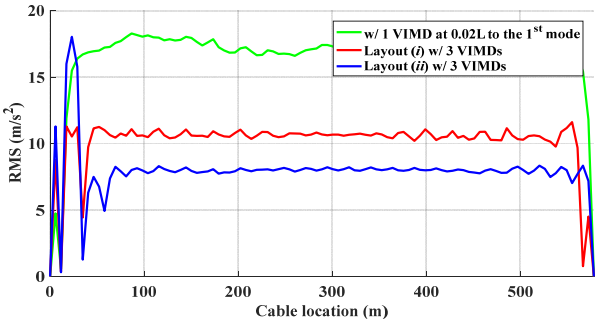

(d) RMS values of the acceleration

Fig. 24 Cable response reduction by multiple VIMDs under random wind load

responses at the 1st natural frequency of the three cases are similar, and the responses at the 2nd frequency of two layouts are remarkably reduced by the 2nd VIMD at 0.98 L and 0.06 L, respectively. Layout (*ii*) shows a better performance of response mitigation at the 5th frequency than that of Layout (*i*). Fig. 23(b) shows the RMS of the displacement along the cable. It can be seen that the responses are effectively reduced by using multiple VIMDs. Compared with the case using one single VIMD, the RMSs of cable displacements using multiple VIMDs are reduced to 40-47% in average.

To simulate a case of cable vibration with high frequency modes, such as in the wind-rain condition, the drag coefficients C_D is artificially taken as 5 for the left one third cable segment while it remains as 1 for the rest cable segment. The random wind velocity fluctuations used in Section 4.4 are considered in this simulation analysis. Figs. 24(a) and (b) show the FAS of the displacements at $x_r = 0.5\,L$ and $0.75\,L$. It can be found that the response at the higher modes are significantly reduced by using multiple VIMDs. Figs. 24(c) and (d) shows the RMSs of cable displacement and acceleration along the cable. Compared with the response using a single VIMD, the RMS values of displacement using multiple VIMDs are reduced to 72% levels by Layout (*i*) and 68% levels by Layout (*ii*) in average, while the RMSs of acceleration are reduced to 61% and 46% levels. It is to be noted that each VIMD is optimized individually to the target cable mode, which makes the design of the multiple VIMDs very simple and straight forward.

Table 9 Modal damping ratios with different tensions

Case	Tension loss	Target mode	Frequency w/o a VIMD (*Hz*)	Split frequency w/ a VIMD (*Hz*)	ξ_n
1.	5%	1st	0.197	0.185	6.76%
				0.216	5.93%
		2nd	0.394	0.371	6.59%
				0.431	5.75%
		3rd	0.591	0.559	6.23%
				0.643	5.21%
2.	10%	1st	0.192	0.18	6.95%
				0.21	6.09%
		2nd	0.383	0.362	6.77%
				0.419	5.9%
		3rd	0.575	0.544	6.41%
				0.625	5.35%
3.	20%	1st	0.181	0.17	7.38%
				0.198	6.43%
		2nd	0.361	0.342	7.2%
				0.394	6.23%
		3rd	0.542	0.515	6.82%
				0.588	5.66%

4.6 Robustness of VIMD design

The robustness of the proposed optimal design of VIMD was investigated for three cases of cable tension losses by 5, 10, and 20%. The super long cable in Section 4.5 was used, and the optimal VIMD parameters (shown in Table 2 with $x_d = 0.02\,L$) remained the same.

Table 9 shows that the cable frequencies as well as the split frequencies decrease with the tension losses. According to Eq. (19), the inertial mass keeps being optimal for the cable with different cable tension, but the damping coefficient and ratios increase slightly compared with those with the original cable tension shown in Table 2.

Fig. 25(a) shows the FRF curves at $x_r = 0.7\,L$ under a sinusoidal load at $x_e = 0.9\,L$ with a VIMD optimized to the 1st mode. As expected, the natural frequencies decrease with the decreased cable tension. Furthermore, the values of both the peak and valley points on the FRF curve increase slightly due to the decreased tension. Fig. 25(b) shows the RMS values of the cable displacements under the random wind load used in Section 4.4. The cable responses increase significantly (up to 25%) mainly due to the decreased cable tension. The VIMD performance with the proposed optimal parameters is found to be fairly robust against the change in the cable property such as the cable tension.

5. Conclusions

We propose a new optimal design method for a VIMD on a taut cable based on the fixed-points method (FPM)

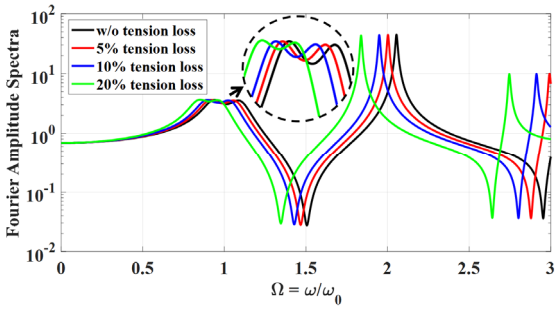

(a) FRF curves at $x_r = 0.7\,L$ for $x_r = 0.9\,L$: optimized to the 1st mode

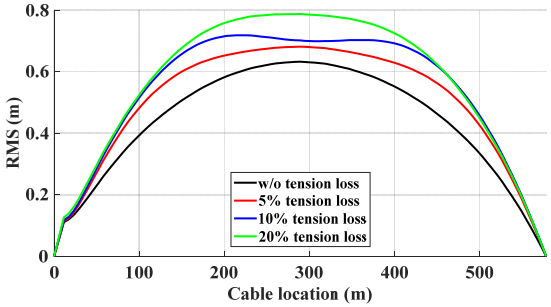

(b) RMS values of displacement

Fig. 25 Robustness of the VIMD for cable tension losses

originally developed for a TMD on conventional structures such as buildings and bridges. The optimal VIMD parameters are derived by considering a cable under a sinusoidal distributed load proportional to the target cable mode. Performance of the VIMD was investigated on the vibration reduction under concentrated sinusoidal loads and distributed random loads. Multiple VIMDs were also studied for multi-modes control. The findings of this study can be summarized as follows:

(1) The target cable mode is split into two vibration modes and the modal damping ratio increases very significantly by introducing a VIMD with a large effective inertial mass similarly to a TMD on an ordinary structure.
(2) Simulation analyses showed that cable vibration can be reduced remarkably by the proposed optimal VIMD or the reference optimal VIMD (to 2-4% levels of cables without a damper under concentrated loads with the resonant frequencies, and to 20-30% and 25-28% levels under distributed random loads and earthquake load, respectively.). Both VIMDs showed negative stiffness characteristics which improve their vibration reduction capability.
(3) The proposed optimal VIMD gave better performance in the response reduction than the reference VIMD, whereas the latter was developed for the maximum modal damping ratios. The difference in vibration reduction is about 35% for a concentrated harmonic load with each resonant frequency and 3-10% for distributed random loads.
(4) Simulation analyses also showed that the multi-modal cable vibrations can be reduced very effectively by using multiple VIMDs. Compared with the responses using a single VIMD, the cable responses can be mitigated to 47% and 40% levels of two layouts using 3 VIMDs under a sinusoidal excitation with multi-components in average, and to 72% and 68% levels by two layouts under a random wind load, respectively.
(5) The proposed optimal design of VIMD is found to be fairly robust to the cable tension changes.

Further studies are suggested for the development of VIMD prototypes, experimental validation on scaled or full-scaled cables, and the further investigation of the interference among the multiple VIMDs.

Acknowledgments

The research described in this paper was financially supported by the National Key R&D Program of China (2018YFE0125400, 2019YFE0112600, 2017YFC0806100) and National Natural Science Foundation of China (U1709216).

References

Bahar, A., Salavati-Khoshghalb, M. and Ejabati, S.M. (2018), "Seismic protection of smart base-isolated structures using negative stiffness device and regulated damping", *Smart Struct. Syst., Int. J.*, **21**(3), 359-371. https://doi.org/10.12989/sss.2018.21.3.359

Batou, A. and Adhikari, S. (2019), "Optimal parameters of viscoelastic tuned-mass dampers", *J. Sound Vib.*, **445**, 17-28. https://doi.org/10.1016/j.jsv.2019.01.010

Brock, J.E. (1946), "A note on the damped vibration absorber", *Transact. Am. Soc. Mech. Engr.*, **13**(4), A284-A284. https://doi.org/10.1115/1.4009588

Cao, Y.H., Xiang, H.F. and Zhou, Y. (2000), "Simulation of stochastic wind velocity field on long-span bridges", *J. Eng. Mech. ASCE*, **126**(1), 1-6. https://doi.org/10.1061/(ASCE)0733-9399(2000)126:1(1)

Christenson, R.E., Spencer Jr, B.F. and Johnson, E.A. (2015), "Experimental verification of smart cable damping", *J. Eng. Mech.*, **132**(3), 268-278. https://doi.org/10.1061/(ASCE)0733-9399(2006)132:3(268)

Den Hartog, J.P. (1934), *Mechanical Vibrations*, McGraw Hill, New York, NY, USA.

Deodatis, G. (1996), "Simulation of ergodic multivariate stochastic processes", *J. Eng. Mech.*, **122**(8), 778-787. https://doi.org/10.1061/(ASCE)0733-9399(1996)122:8(778)

Duan, Y.F., Ni, Y.Q., Zhang, H.M., Spencer Jr, B.F., Ko, J.M. and Fang, Y. (2019a), "Design formulas for vibration control of taut cables using passive MR dampers", *Smart Struct. Syst., Int. J.*, **23**(6), 521-536. https://doi.org/10.12989/sss.2019.23.6.521

Duan, Y.F., Ni, Y.Q., Zhang, H.M., Spencer Jr, B.F., Ko, J.M. and Dong, S.H. (2019b), "Design formulas for vibration control of sagged cables using passive MR dampers", *Smart Struct. Syst., Int. J.*, **23**(6), 537-551. https://doi.org/10.12989/sss.2019.23.6.521

Duan, Y.F., Chen, Q.Y., Zhang, H.M., Yun, C.B., and Zhu, Q. (2019c), "CNN-based damage identification method of tied-arch bridge using spatial-spectral information", *Smart Struct. Syst., Int. J.*, **23**(5), 507-520. https://doi.org/10.12989/sss.2019.23.5.507

Fujino, Y. and Hoang, N. (2008), "Design formulas for damping of a stay cable with a damper", *J. Struct. Eng.*, **134**(2), 269-278. https://doi.org/10.1061/(ASCE)0733-9445(2008)134:2(269)

Gao, H., Wang, H., Li, J., Wang, Z., Liang, R., Xu, Z. and Ni, Y. (2019), "Optimum design of viscous inerter damper targeting multi-mode vibration mitigation of stay cables", *Eng. Struct.*, **226**, 111375. https://doi.org/10.1016/j.engstruct.2020.111375

Garrido, H., Curadelli, O. and Ambrosini, D. (2013), "Improvement of tuned mass damper by using rotational inertia through tuned viscous mass damper", *Eng. Struct.*, **56**, 2149-2153. https://doi.org/10.1016/j.engstruct.2013.08.044

Høgsberg, J. (2011), "The role of negative stiffness in semi-active control of magneto-rheological dampers", *Struct. Control Health Monitor.*, **18**(3), 289-304. https://doi.org/10.1002/stc.371

Hua, Y., Wong, W. and Cheng, L. (2018), "Optimal design of a beam-based dynamic vibration absorber using fixed-points theory", *J. Sound Vib.*, **421**, 111-131. https://doi.org/10.1016/j.jsv.2018.01.058

Iemura, H. and Pradono, M.H. (2010), "Simple algorithm for semi-active seismic response control of cable-stayed bridges", *Earthq. Eng. Struct. Dyn.*, **34**(4-5), 409-423. https://doi.org/10.1002/eqe.440

Ikago, K., Saito, K. and Inoue, N. (2012a), "Seismic control of single-degree-of-freedom structure using tuned viscous mass damper", *Earthq. Eng. Struct. Dyn.*, **41**(3), 453-474. https://doi.org/10.1002/eqe.1138

Ikago, K., Sugimura, Y., Saito, K. and Inoue, N. (2012b), "Modal

response characteristics of a multiple-degree-of-freedom structure incorporated with tuned viscous mass dampers", *J. Asian Architect. Build. Eng.*, **11**(2), 375-382. https://doi.org/10.3130/jaabe.11.375

Jamshidi, M., Chang, C.C. and Bakhshi, A. (2017), "Self-powered hybrid electromagnetic damper for cable vibration mitigation", *Smart Struct. Syst., Int. J.*, **20**(3), 285-301. https://doi.org/10.12989/sss.2017.20.3.285

Javanbakht, M., Cheng, S. and Ghrib, F. (2018), "Refined damper design formula for a cable equipped with a positive or negative stiffness damper", *Struct. Control Health Monitor.*, **25**(10), e2236. https://doi.org/10.1002/stc.2236

Jeong, S., Lee, J., Cho, S. and Sim, S. (2019), "Integrated cable vibration control system using Arduino", *Smart Struct. Syst., Int. J.*, **23**(6), 695-702. https://doi.org/10.12989/sss.2019.23.6.695

Johnson, E.A., Spencer Jr, B.F. and Fujino, Y. (1999a), "Semiactive damping of stay cables: A preliminary study", *Proceedings of the 1999 17th International Modal Analysis Conference* (*IMAC*), Kissimmee, FL, USA, pp. 417-423.

Johnson, E.A., Baker, G.A., Spencer Jr, B.F. and Fujino, Y. (1999b), "Semiactive damping of stay cables", *J. Eng. Mech.*, **133**(1), 1-11. https://doi.org/10.1061/(ASCE)0733-9399(2007)133:1(1)

Kovacs, I. (1982), "Zur Frage der Seilschwingungen und der seildämpfung", *Bautechnik*, **10**, 325-332.

Krenk, S. (2000), "Vibrations of a taut cable with an external damper", *J. Appl. Mech.*, **67**(4), 772-776. https://doi.org/10.1115/1.1322037

Krenk, S. (2005), "Frequency analysis of the tuned mass damper", *J. Appl. Mech.*, **72**(6), 936-942. https://doi.org/10.1115/1.2062867

Krenk, S. and Høgsberg, J. (2009), "Optimal resonant control of flexible structures", *J. Sound Vib.*, **323**(3-5), 530-554. https://doi.org/10.1016/j.jsv.2009.01.031

Krenk, S. and Nielsen, S.R.K. (2002), "Vibrations of a shallow cable with a viscous damper", *Proceedings of the Royal Society A-Mathematical, Physical and Engineering Sciences*, **458**(2018), 339-357. https://doi.org/10.1098/rspa.2001.0879

Li, H., Liu, M. and Ou, J.P. (2008), "Negative stiffness characteristics of active and semi-active control systems for stay cables", *Struct. Control Health Monitor.*, **15**(2), 120-142. https://doi.org/10.1002/stc.200

Liu, K. and Liu, J. (2005), "The damped dynamic vibration absorbers: revisited and new result", *J. Sound Vib.*, **284**(3-5), 1181-1189.

Lu, L., Duan, Y.F., Spencer Jr, B.F., Lu, X.L. and Zhou, Y. (2017), "Inertial mass damper for mitigating cable vibration", *Struct. Control Health Monitor.*, **24**(10), 1-12. https://doi.org/10.1002/stc.1986

Lu, L., Fermandois, G.A., Lu, X.L., Spencer Jr, B.F. and Zhou, Y. (2019), "Experimental evaluation of an inertial mass damper and its analytical model for cable vibration mitigation", *Smart Struct. Syst., Int. J.*, **23**(6), 589-613. https://doi.org/10.12989/sss.2019.23.6.589

Marian, L. and Giaralis, A. (2017), "The tuned mass-damper-inerter for harmonic vibrations suppression, attached mass reduction, and energy harvesting", *Smart Struct. Syst., Int. J.*, **19**(6), 665-678. https://doi.org/10.12989/sss.2017.19.6.665

Ministry of Transport of the People's Republic of China (2018), *Wind-resistant Design Specification for High Way Bridges*, JTG/T 3360-01-2018.

Nakamura, Y., Fukukita, A., Tamura, K., Yamazaki, I., Matsuoka, T., Hiramoto, K. and Sunakoda, K. (2014), "Seismic response control using electromagnetic inertial mass dampers", *Earthq. Eng. Struct. Dyn.*, **43**(4), 507-527. https://doi.org/10.1002/eqe.2355

Ni, Y.Q., Duan, Y.F., Chen, Z.Q. and Ko, J.M. (2002), "Damping identification of MR-damped bridge cables from in-situ monitoring under wind-rain-excited conditions", *Proceedings of the Society of Photo-optical Instrumentation Engineers* (*SPIE*), **4696**, 41-51. https://doi.org/10.1117/12.472573

Ozer, M.B. and Royston, T.J. (2005), "Extending Den Hartog's vibration absorber technique to multi-degree-of-freedom systems", *J. Vib. Acoust.*, **127**(4), 341-350. https://doi.org/10.1115/1.1924642

Pacheco, B.M., Fujino, Y. and Sulekh, A. (1993), "Estimation curve for modal damping in stay cables with viscous damper", *J. Struct. Eng. ASCE*, **119**(6), 1961-1979. https://doi.org/10.1061/(ASCE)0733-9445(1993)119:6(1961)

Ren, M.Z. (2001), "A variant design of the dynamic vibration absorber", *J. Sound Vib.*, **245**(4), 762-770. https://doi.org/10.1006/jsvi.2001.3564

Shen, Y., Peng, H., Li, X. and Yang, S. (2017), "Analytically optimal parameters of dynamic vibration absorber with negative stiffness", *Mech. Syst. Signal Process.*, **85**, 193-203. https://doi.org/10.1016/j.ymssp.2016.08.018

Shum, K.M. (2009), "Closed form optimal solution of a tuned liquid column damper for suppressing harmonic vibration of structures", *Eng. Struct.*, **31**(1), 84-92. https://doi.org/10.1016/j.engstruct.2008.07.015

Shi, X. and Zhu, S.Y. (2015), "Magnetic negative stiffness dampers", *Smart Mater. Struct.*, **24**(7), 072002. https://doi.org/10.1088/0964-1726/24/7/072002

Shi, X. and Zhu, S.Y. (2018), "Dynamic characteristics of stay cables with inerter dampers", *J. Sound Vib.*, **423**, 287-305. https://doi.org/10.1016/j.jsv.2018.02.042

Simiu, E. and Scanlan, R.H. (1996), *Wind Effects on Structures: Fundamentals and Applications to Design*, (Third Edition), John Wiley & Sons, Inc., New York, NY, USA.

Spencer Jr, B.F., Dyke, S.J., Sain, M.K. and Carlson, J.D. (1997), "Phenomenological model for magnetorheological dampers", *J. Eng. Mech. ASCE*, **123**(3), 230-238. https://doi.org/10.1061/(ASCE)0733-9399(1997)123:3(230)

Wang, M., Sun, F., Yang, J. and Nagarajaiah, S. (2019), "Seismic protection of SDOF systems with a negative stiffness amplifying damper", *Eng. Struct.*, **190**, 128-141. https://doi.org/10.1016/j.engstruct.2019.03.110

Weber, F. and Distl, H. (2015), "Semi-active damping with negative stiffness for multi-mode cable vibration mitigation: approximate collocated control solution", *Smart Mater. Struct.*, **24**(11), 115015. https://doi.org/10.1088/0964-1726/24/11/115015

Wong, W.O., Fan, R.P. and Cheng, F. (2018), "Design optimization of a viscoelastic dynamic vibration absorber using a modified fixed-points theory", *J. Acoust. Soc. Am.*, **143**(2), 1064-1075. https://doi.org/10.1121/1.5024506

Zhu, X., Chen, Z. and Jiao, Y. (2018), "Optimizations of distributed dynamic vibration absorbers for suppressing vibrations in plates", *J. Low Freq. Noise Vib. Active Control*, **37**(4), 1188-1200. https://doi.org/10.1177/1461348418794563

HJ